Lund University

LTH — FACULTY OF ENGINEERING

Department of Energy Science

Master degree in Energy Engineering — Renewables energies

LUND UNIVERSITY

Modeling of the trajectory of ice thrown from a wind turbine

Supervisor

Robert-Zoltán SZÁSZ

Examiner

Johan REVSTEDT

Elena ROCCHI

Academic year 2022-2023

Ai miei genitori e alla mia famiglia,
senza di voi tutto questo sarebbe rimasto solo un’idea.

Abstract

There is a growing number of wind turbines installed in cold temperature zones as a result of the restricted space for new construction. Due to ice deposition on the turbine blades, the increasing installation of wind turbines in freezing temperature areas presents many challenges: ice accumulation increases weight, unbalances the rotor, diminishes aerodynamic efficiency, and creates safety issues.

This paper attempts to investigate the influence of the velocity magnitude and Reynolds number on aerodynamic forces, given by Drapalik et al. [6], for different ice concretions.

Moreover, it will be examined how the sensitivity of the forces are modified based on different turbulence models through RANS and LES simulations. RANS models included the SST k-ω, RNG k-ε, Realizable k-ε, and Spalart-Allmaras models, while the WALE SGS model was used for LES simulations to capture small-scale fluid motions.

Lastly, the ice trajectories were evaluated based on the in-house ballistic model, while considering different resolution of the aerodynamic force database acting on the ice.

Preface

This master's thesis has been elaborated thanks to the Erasmus programme, developed between my home university, the Universitat Politècnica de Catalunya, and my host, the Lund University, specifically, the Energy Science department; and has been one of the best opportunities of my life. It has allowed me to widen my views and examine the intriguing area of fluid dynamics, a discipline related to my studies in energy engineering while realizing my dream of studying in Sweden.

This thesis represents the culmination of years of passionate study, endless periods of frustration and wrong results, and countless hours of hard work. Nevertheless, it is with great pride and a sense of accomplishment that I present this thesis to the academic community.

I would like to express my sincere gratitude to my thesis advisor, Robert-Zoltán Szász, for his consistent support, invaluable guidance, and expertise throughout this entire research venture. His mentorship has been fundamental in shaping the direction and scope of this study, pushing me to strive for excellence in my work.
I would also like to extend my appreciation to the faculty members of the Energy Science Department for their contributions to my academic growth.

Finally, I would like to acknowledge the support and encouragement from my family and friends: their resolute belief in my abilities and their constant encouragement have been a source of motivation during these challenging times. First of all my friends from my bachelor studies and from home, the most phenomenal people that I know that kept me motivated and helped me throughout the challenges of studying abroad.
Then all the wonderful people that I met during my years at UPC that reaffirmed in me the passion for science that I thought I had lost.
Finally yet importantly, all the friends that I have made in this Erasmus, which reminded me how stimulating is to meet people from all over the world.

Elena Rocchi
Lund University - Universitat Politècnica de Catalunya
05.06.2023

Index

1. Introduction

Wind power has emerged as an important source of renewable energy, offering a sustainable alternative to traditional fossil fuel-based electricity generation.
Onshore wind turbines, a common feature in many regions, utilize the power of wind to generate clean and environmentally friendly electricity. However, among the numerous advantages of wind power, there are some challenges associated with the accumulation of ice on the turbine blades, which can result in ice falling from the turbines.
This phenomenon brings risks to both the windmill themselves and the surrounding environment, necessitating careful consideration and effective mitigation measures.

In colder climates and areas with inclement weather, where wind energy represents an increasing part of the production of electricity, such as Nordic countries and high-altitude areas; the build-up of ice on wind turbine blades is a frequent occurrence.

When ambient temperatures drop below freezing, moisture in the air can condense and freeze upon contact with the turbine surfaces, leading to ice formation. Over time, this ice can accumulate on the blades, affecting their aerodynamic performance and introducing imbalances that may stress the turbine's mechanical components.

The issue of ice falling from wind turbine blades is a multifaceted concern that requires attention due to the potential threats it poses. Unlike stationary structures, icing on rotating turbines is more complex. Since the ice formation process depends on the relative air velocity, more ice forms towards the tip of the blade. Differently from ice fragments that fall from buildings and pylons, which usually start from a stationary state, ice ejected from a rotating wind turbine has a constant initial velocity.

Falling ice from turbine blades can put in danger the safety of workers performing maintenance or repair tasks in wind farms, as well as individuals living or working in close proximity to these structures.

Moreover, the impact of ice fragments or chunks falling from a height can inflict damage on nearby structures, such as buildings, vehicles, or infrastructures. This risk emphasises the importance of effective mitigation measures to prevent ice shedding and ensure the protection of both property and human lives.

Efforts to address the challenge of icing on wind turbine blades and the subsequent ice shedding, have led to the implementation of various strategies by turbine manufacturers and operators. These strategies aim to minimize ice formation and mitigate the risks associated with ice falling from the blades.

De-icing and anti-icing systems, including heating elements or coatings, are commonly employed to prevent or remove ice build-up. Additionally, sensors and monitoring systems are used to detect ice accumulation and facilitate timely action. Regular inspections, maintenance protocols, and clear safety guidelines are also crucial to ensure the safe operation of wind turbines in icy conditions.[1].

1.2 Short background

The design and implementation of wind farms require careful consideration of various factors to ensure their safe and efficient operation. Among these considerations, the issue of ice throw or fall from wind turbines is a crucial aspect that demands analysis and prediction.

Ice throw refers to the ejection of ice fragments from rotating turbine blades, while ice fall relates to the detaching of ice from the blades that subsequently drops to the ground.
These two topics have been extensively studied in numerous research projects, which have examined different types of ice models, various techniques to analyse ice accumulation, and suggested prediction tools to forecast the trajectories for ice throw and fall.

Initially the simulation models in the scientific literature, started considering a spherical ice shape falling from stationary structures during adverse weather condition.
This choice was motivated due to its simplicity for the computation of the trajectory and because of pre-existent data used for ice concretion falling from bridges or static structures.
Later on, Raeesi et al. [2] tried to improve the model by working with a semi-cylindrical shape instead of a spherical one but still focusing on static infrastructures.

However, it has been found that the trajectory of the ice depends mostly on the wind speed and direction than the shape of the ice concretion. The aspect ratio (height/radius), in particular, has the most effect on the aerodynamic forces and moments.
In fact, independently from the shape of the ice, the maximum throwing distance introduced by Seifert et al, (2003) was assumed to be as in *Equation 1*:

$$d = 1{,}5 \cdot (D + H) \qquad (1)$$

Considering d as the throwing distance, D the rotor diameter and H the hub height.
The main limitation of this equation is its lack of sensitivity to wind conditions, resulting in a throwing distance that remains unaffected by the wind.
Consequently, the probability area for ice throw, when using this method, would form a circular shape and be larger than what would occur in reality. As a result, this can be considered a worst-case scenario.

Due to the low accuracy of this analysis and its lack of information for rotating systems, another further accurate scientific article has been evaluated.

It focuses on the ice accretion modeled as half of a cave cylinder, with a C-section and using a grid structure to study the trajectory and the forces [3].
The forces and moments acting on the ice were computed using a 6 DOF (Degree of Freedom) trajectory solver. The aerodynamic forces and moments were pre-computed using CFD-simulations and then interpolated depending on the instantaneous relative speed.

In order to have a more precise description of the trajectory and to estimate the highest falling probability area, a more realistic flat-shaped model was examined.
In this study, the influence of the mass of the ice fragment, the position of it on the blade, the drag coefficient, rotor speed and wind speed were proven to influence significantly the throwing distance of the ice. [4]

Finally, because these were all simulations of hypothetical trajectories and behaviours, a real experiment has been investigated: in Drapalik et al. [5], the researchers collected ice fragments fallen from a wind turbine and prepared realistic 3D replicas, adjusting the density of the model to match the density of the ice.

After that, the samples were then launched using a device that acted as a miniature wind turbine, and then they reconstructed the trajectory in a three-dimensional model and compared it with a ballistic model, finding many differences.
It is evident that drag forces play a crucial role in determining velocity and maximum distance, so the hypothesis to neglecting these forces is not viable.
Furthermore, when comparing the simulation results with established ballistic models, notable disparities are observed.

Further assessment and additional studies are needed to demonstrate the consequences of the variation of additional parameters ensuring a comprehensive study of the phenomenon.
Additionally, the experimental observations primarily focus on analysing ice pieces after the fall, but this method is lacking accuracy due to the unknown initial conditions: when and where did the ice detach from? Although another option is to observe ice fall on site, this idea is challenging due to hostile meteorological conditions and safety considerations.

1.3 Objectives

This study aims to address the gaps in previous research by investigating the effects of the Reynolds number on the aerodynamic forces on realistic ice chunks, while also exploring different turbulence models to study the consequences on the accuracy of the force field; furthermore, it seeks to examine the sensitivity of the trajectories.

Specifically, we based our work on the forces and moments database created by Drapalik et al. [7], since it is detailed and determined for realistic ice shapes.

Although in theory it would be possible to find the trajectory of the ice using CFD, such computation would be very demanding. Therefore, the common option is to calculate the forces and moments prior to the ice trajectory.
However, these pre-computations can be computationally intensive. To optimize resource usage, a potential solution is to normalize the forces using the square of the wind speed (U^2), which reduces the number of required calculations.

Nonetheless, one needs to assess the errors associated to this approach, and, additionally, the choice of turbulence modeling is critical, considering cost factors (such as comparing Large Eddy Simulation (LES) and Reynolds-Averaged Navier-Stokes (RANS) models and the limitations associated with them) and accuracy factors as well.

RANS models have limitations and cannot be expected to yield accurate predictions in all circumstances. By exploring various RANS models, the study aims to address the turbulence-modeling sensitivity of the predicted forces.

In summary, the paper will be structured based on the following set of questions:

I. What is the impact of the Reynolds number on the aerodynamic forces acting on the ice? What is the error if the aerodynamic forces are normalized with respect to the relative speed?
I. What is the impact of turbulence modeling? Commonly, aerodynamic forces are determined using Reynolds Averaged Navier Stokes (RANS) based methods. Here, we will test several RANS models and investigate the impact of using Large Eddy Simulation (LES) for selected orientations of the ice.
II. What is the impact of the investigated parameters on the sensitivity of trajectory computations?

2. Case description

As previously mentioned in the introductive section, obtaining experimental data for trajectory validations can be challenging due to various factors.
On-site observations present difficulties in terms of timing and safety, and precise measurements require careful judgment and can be dangerous. The option of determining the precise origin and condition of the ice after it falls on-site is also problematic, and lastly, conducting experiments in climatic wind tunnels, while valuable, can be cost-prohibitive.

To overcome all these challenges, Drapalik et al. [5] employed an innovative approach: they utilized 3D scanning to capture real ice pieces and subsequently created 3D printed replicas, adjusting their density to achieve accurate representations. By conducting measurements under controlled conditions, they obtained reliable data.
Furthermore, they developed a precomputed force database, expanding the accuracy of their findings. This methodology made a significant contribution to the field by providing realistic and controlled measurements for trajectory analysis.

This study started by manipulating on the database given by Drapalik et al. [7] that collected the forces and the momentum for different ice shapes. In this paper, we will focus on the two most relevant shapes to our study: DAV, DAD; while considering the initial wind speed variation as $U_{x,y,z}$=[-40,40].

Figures 1 and 2 show the concretions displayed in their reference system.

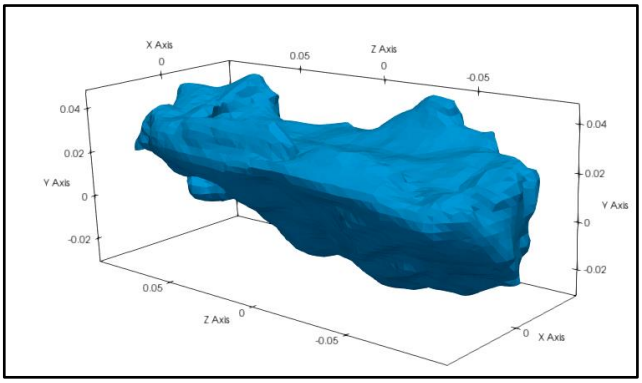

Figure 1 – DAV ice shape

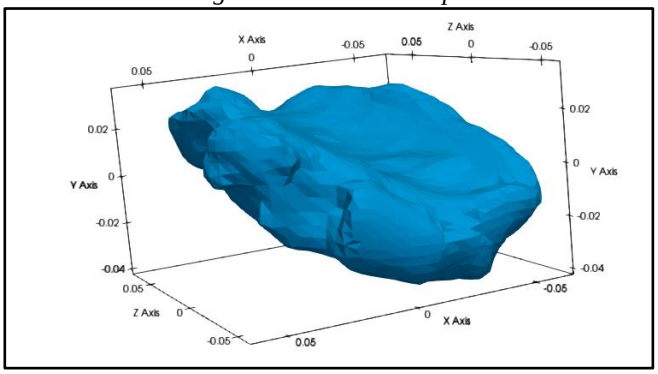

Figure 2 – DAD ice shape

3. Reynolds number effect

For each of the three velocity components, Purker et al. [7] created a complete database with 81x81x81 data points that spans the range of U=[-40; 40]m/s.
At the start of the project, some cases have been interpolated, but not all of them because it would have been too time-consuming. It is debatable whether including all the data points is necessary, or whether normalization and rescaling may be used instead.

To evaluate the relevance of velocity magnitude (and subsequently Reynolds number, Re), the forces have been divided by its square, since the aerodynamic force is directly proportional to the square of velocity.

The Reynolds number is defined, in *Equation 2*:

$$Re\ [-] = \frac{F_{inertial}}{F_{viscous}} = \frac{\rho u L}{\mu} \qquad (2)$$

Considering:

- ρ $\left[\frac{kg}{m^3}\right]$ - density of air
- u $\left[\frac{m}{s}\right]$ - initial speed at the inlet of the mesh
- L $[m]$ - prevailing size of ice
- μ $\left[\frac{kg}{m \cdot s}\right]$ - dynamic viscosity of air

3.1 Model description

Within the EISBALL project [5] the before-mentioned force database was available and has been modified as following, starting from the generic formulation of the aerodynamic force as in *Equation 3*:

$$F_{areodynamic} = \frac{1}{2} \cdot C_1 \cdot \rho_{air} \cdot A \cdot U^2 \tag{3}$$

Considering

$$C_2 \left[\frac{kg}{m}\right] = \frac{1}{2} \cdot C_1 \cdot \rho_{air} \cdot A \; ; \tag{4}$$

$$F_{normalized}\,[-] = \frac{F_a}{C_2 \cdot U^2} \tag{5}$$

Since the idea is to test the Re-number dependence, by normalizing the force it is been tested the dependence on the coefficient C_1, that is expected to be constant. Then, it has been plotted:

$$\overline{\boldsymbol{F}}_{\boldsymbol{norm}} = \frac{\sqrt{F_x^2+F_y^2+F_z^2}}{\|U^2\|} \tag{6}$$

A constant value of F_{norm} in radial direction indicates that F_{norm} is not dependent on the Reynolds number thus; is not needed to pre-compute the forces in several points along that line.

3.2 Results

As commented before in 3.1 Model description, the aerodynamic forces have been normalized by dividing them for the square velocity, to assess how much the force coefficient obtained in this manner depends on the velocity magnitude. All of these calculations were made directly in Paraview manipulating the database.
In *Figure 3* is depicted the normalized database: on the axes, it has been plotted the relative velocity, setting the lower speeds in the centre and, consequently, having the highest values at the sides of the cube.

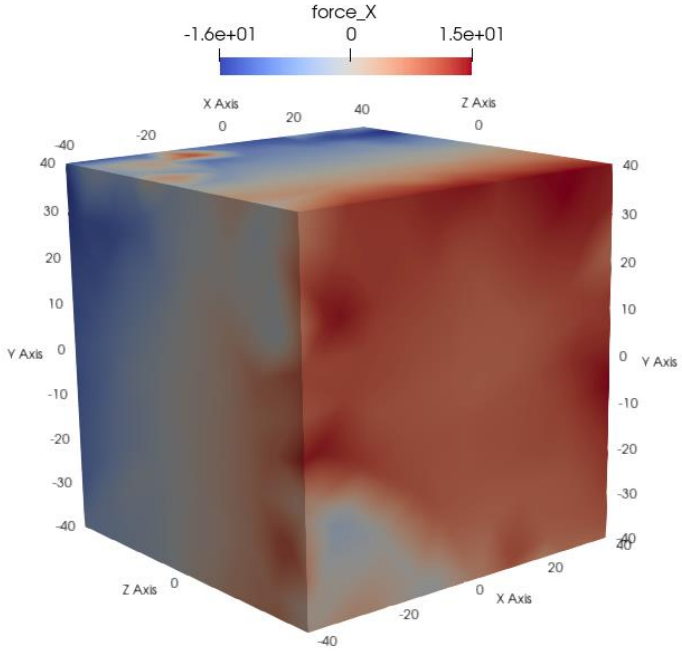

To picture how the forces behave as function of the relative velocity, the section in the F_{Uz}=0-plane was considered, for the different ice concretions placed in the mesh.

In order to evaluate the azimuthal variation of the forces, the evolution of the force was studied along the eight different directions in which the section was split, following the radial division, as shown in *Figure 4*.

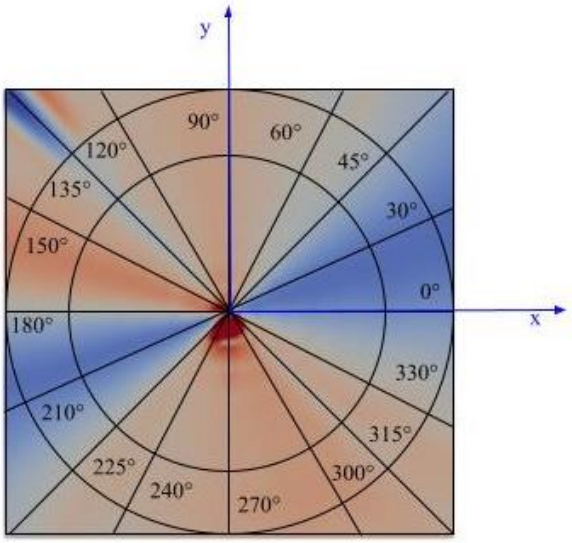

Figure 4 – Radial division considered

So that the speed follows a growing pattern, a point close to the centre has low velocity while one far away has higher. Hence, for instance, the top right corner of *Figure 4* corresponds to the relative velocity U_{rel}= (40, 40, 0).

Figure 5 shows the normalized force in the U_z=0 m/s plane obtained for the DAD ice in the 30° direction and the centre of the figure corresponds to zero relative velocity.

It can be observed that there are significant variations in the azimuthal direction as expected, since the ice does not have a spherical shape and different orientations of the relative velocity should result in different magnitudes of the aerodynamic forces.

On the other hand, the variations in radial direction are minor, except for low (<5 m/s) velocity magnitudes (close to the figure centre). This indicates, that the normalized forces depend on the Re number only for low velocity values.

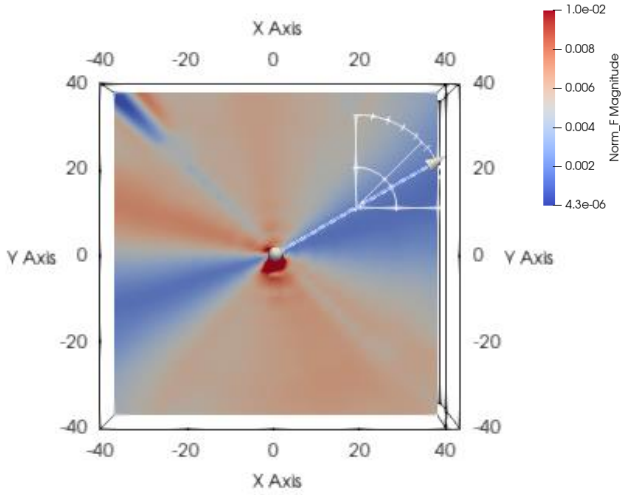

Figure 5 – Section of Uz=0 of the normalized forces for the DAD ice shape

Due to its concave shape, above and below the depressed area, the forces increase significantly because of the higher turbulence of the region.

Moreover, two different areas can be distinguished: from 0° to 60° the effect of the forces is lower for the wake effect generated by the shape of the object, while from 60° to 180° they increase again. The pattern is then repeated in the third and fourth quadrant of the section in *Figure 5*.

Compared to the other figure seen before, the DAV ice concretion is more symmetrical (see *Figure 6*), as it can be deduced from the forces distribution in the section.
As is it portrayed, two areas can be distinguished:

- $\bar{F} < 0.006$ in the region of (-30°, 60°) and again (120°, 225°)
- $\bar{F} > 0.006$ elsewhere.

This pattern was expected because the shape resembles a lot the one of a flat plane surrounded by an airflow so the forces need to have a repetitive behaviour similarly to the already-known base case.

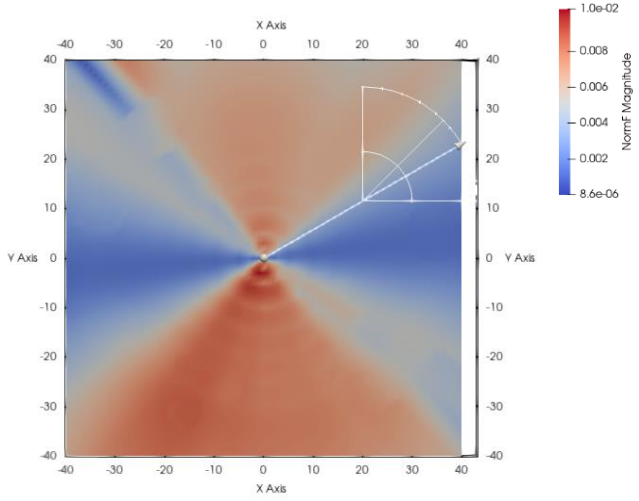

Figure 6– Section of Uz=0 for the DAV ice shape

Considering a quantitative point of view, from the comparison of the different forces respect to the normalized speed and plotting in function of the different values of the speed; the normalized force in the region in which U≤5m/s, is clearly higher for the DAD ice shape compared to the DAV one.

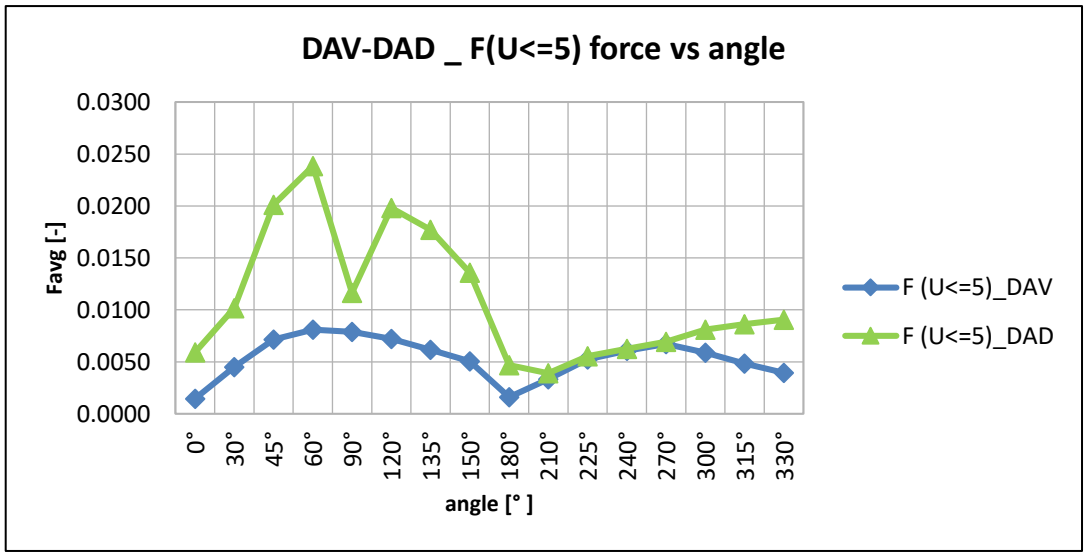

Figure 7 – Normalized force for speed lower than 5 m/s

Meanwhile, when the velocity increases the force profiles tends to have a similar trend despite the different ice concretions shapes.

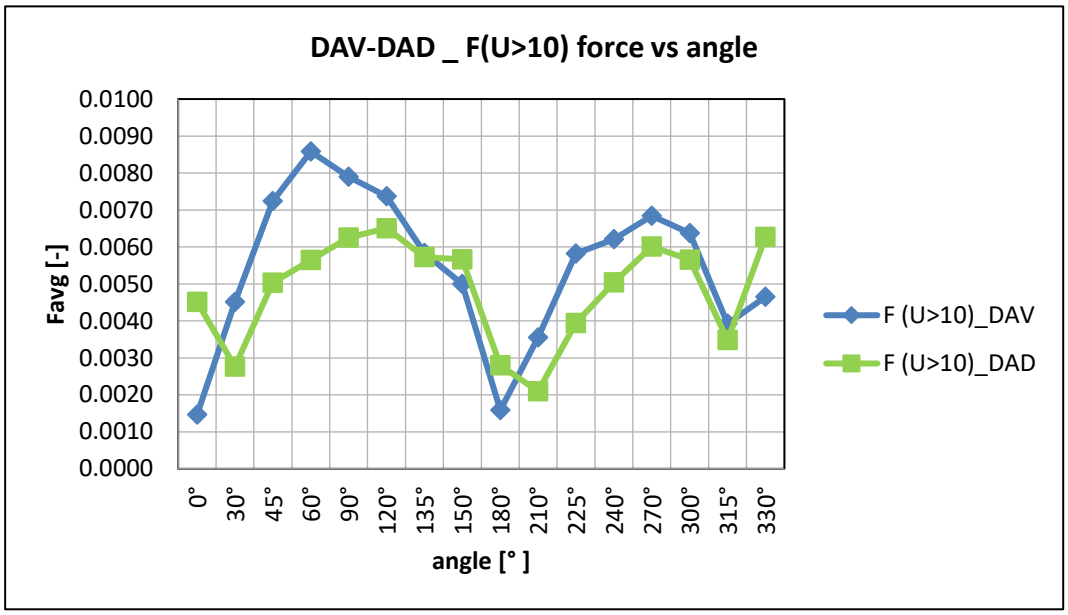

Figure 8 – Normalized force for speed higher than 10 m/s

3.3 Conclusion

As portrayed in the 3.2 Results paragraph, the variation in the speed profiles is noticeable when it is lowered down to the 5m/s section, and the differences are highlighted between the DAD and DAV ice concretions.

First of all, as said before, the DAD ice-shape is the most irregular and anti-symmetric one so is evident that the speed field will behave consequently when investing the object considered.

In addition to the above, the change of the force behaviour is observable when the speed is very low, so in the laminar region where the Reynolds number is less reliable because of its easy variation. Accordingly, the higher sensitivity to Re number at low velocity magnitudes was expected.

As a matter of fact, in the transient region, where the Re-number is still low and the vortexes start to form, the turbulence flow is not completely developed and, at the same time, is not possible to consider laminar flow due to the high Reynolds. For this reason, the RANS model used cannot interpret accurately the flow development.
Therefore, in the results, it can be detected discontinuity in the force pattern.

In contrast, it can be concluded that the speeds, and, as a consequence, the Reynolds number, do not have a direct effect on the normalized forces for relative speeds larger than 5 m/s.
In fact, as showed in *Figure 7* and *8*, their behaviour remains almost completely unaltered in between the two ice shapes.

4. Turbulence models effects

The database generated by Drapalik [6] was obtained using the k-ω SST RANS model.

Since RANS models cannot be expected to be case independent, the goal of this work was to assess the sensitivity of the predicted aerodynamic forces on the choice of turbulence model.
The study has been initially implemented in OpenFOAM through different RANS models to observe the consequence of the different computation methods on the output of the simulations. The results will then be compared to the data reported in [5].
For the CFD computations, OpenFOAM [8] will be used. The impact of turbulence modeling on the ice trajectories will be evaluated using the models reported in [5] and/or [6].

Afterwards, for selected condition(s), where the RANS results indicated difficulties to converge, LES simulations have been run, and are being expected to have a higher accuracy.

4.1 Model description

To compute the RANS simulations, mainly the *simpleFoam* [9] solver was employed because of it is incompressible and steady-state condition and its ability to solve relatively quickly turbulent flows. In particular, in Annex I there is the detail of the *fvSolution* the controller of the equation solvers, tolerances and algorithms and the *fvSchemes*, showing the discretization schemes.

Whereas, for LES simulations, *pimpleFoam* [10] was the best option since it allowed a larger time-step transient solver while still considering incompressible flows, as for RANS, the model details are depicted in the *fvSolution* and *fvSchemes* in the Annex I.

I. RANS turbulence models

I. Shear stress transport model - SST $k-\omega$

The Shear Stress Transport model is a variant of the standard k–ω model that combines the standard k–ω model and the equations of k–ε model; using the first near the walls, and the other elsewhere. Therefore is a two-equation model that also includes a viscosity limitation that helps the model to converge [11]:

$$\begin{cases} \dfrac{\partial k}{\partial t} + U_j \dfrac{\partial k}{\partial x_j} = P_k - \beta^* k\omega + \dfrac{\partial}{\partial x_j}\left[(\nu + \sigma_k \nu_T)\dfrac{\partial k}{\partial x_j}\right] \\ \dfrac{\partial \omega}{\partial t} + U_j \dfrac{\partial \omega}{\partial x_j} = \alpha S^2 - \beta\omega^2 + \dfrac{\partial}{\partial x_j}\left[(\nu + \sigma_\omega \nu_T)\dfrac{\partial \omega}{\partial x_j}\right] + 2(1-F_1)\sigma_{\omega 2}\dfrac{1}{\omega}\dfrac{\partial k}{\partial x_i}\dfrac{\partial \omega}{\partial x_i} \\ \mu_t = \dfrac{\rho a_1 k}{max(a_1\omega, \Omega F_2)} \end{cases} \quad (7)$$

Advantages

Is a two-in-one model since we are using k-ε and k-ω together; the use of a k-ω formulation in the inner parts of the boundary layer makes the model directly meaningful all the way down to the wall through the viscous sub-layer. Hence, the SST k-ω model can be used as a low-Re turbulence model (so without applying any wall function) without any extra damping functions.

Disadvantages

The SST k-ω model, due to its dependency on wall distance, produces a bit too large turbulence levels in regions with large normal strain, like stagnation regions and regions with strong acceleration. Therefore, a Reynolds-stress-model may be more appropriate for flows with sudden changes in strain rate or rotating flows, while the SST model may be more appropriate for separated flows [12].

II. Re-normalization group - RNG $k-\varepsilon$

The re-normalization group model was created by standardizing the Navier-Stokes equations in order to take into account the effects of motion at smaller scales.
The epsilon equation is changed by the RNG approach, a mathematical method that can be used to develop a turbulence model related to the k-ε that tries to account for the various scales of motion by alterations to the production term.
The formulation is again a two-equations-model in which the buoyancy is neglected:

$$\begin{cases} \frac{\partial}{\partial t}(\rho k) + \frac{\partial}{\partial x_i}(\rho k u_i) = \frac{\partial}{\partial x_j}\left[\left(\mu + \frac{\mu_t}{\sigma_k}\right)\frac{\partial k}{\partial x_j}\right] + P_k - \rho\epsilon \\ \frac{\partial}{\partial t}(\rho \epsilon) + \frac{\partial}{\partial x_i}(\rho \epsilon u_i) = \frac{\partial}{\partial x_j}\left[\left(\mu + \frac{\mu_t}{\sigma_\epsilon}\right)\frac{\partial \epsilon}{\partial x_j}\right] + C_{1\epsilon}\frac{\epsilon}{k}P_k - C_{2\epsilon}^{*}\rho\frac{\epsilon^2}{k} \\ C_{2\epsilon}^{*} = C_{2\epsilon} + \frac{C_\mu \eta^3(1-\eta/\eta_0)}{1+\beta\eta^3} \end{cases} \tag{8}$$

Advantages
It accounts for the effects of smaller scales of motion. Since in the standard k-ε model the eddy viscosity is determined from a single turbulence length scale, the calculated turbulent diffusion is the one that occurs only at the specified scale. Whereas, in reality, all scales of motion will contribute to the turbulent diffusion.

Disadvantages
There are no improvements over the standard model for predicting vortex evolution. This model is usually used for indoor air simulations [13].

III. Realizable $k-\varepsilon$

The term "realizable" means that the model satisfies certain mathematical constraints on the Reynolds stresses, consistent with the physics of turbulent flows, given that neither the standard k-ε model nor the RNG k-ε model are realizable [14].
Once again, is a two-equations model:

$$\begin{cases} \frac{\partial}{\partial t}(\rho k)+\frac{\partial}{\partial x_j}(\rho k u_j)=\frac{\partial}{\partial x_j}\left[\left(\mu+\frac{\mu_t}{\sigma_k}\right)\frac{\partial k}{\partial x_j}\right]+P_k+P_b-\rho\epsilon-Y_M+S_k \\ \frac{\partial}{\partial t}(\rho\epsilon)+\frac{\partial}{\partial x_j}(\rho\epsilon u_j)=\frac{\partial}{\partial x_j}\left[\left(\mu+\frac{\mu_t}{\sigma_\epsilon}\right)\frac{\partial \epsilon}{\partial x_j}\right]+\rho\, C_1 S\epsilon-\rho\, C_2\frac{\epsilon^2}{k+\sqrt{\nu\epsilon}}+C_{1\epsilon}\frac{\epsilon}{k}C_{3\epsilon}P_b+S_\epsilon \\ C_1=\max\left[0.43,\frac{\eta}{\eta+5}\right], \quad \eta=S\frac{k}{\epsilon}, \quad S=\sqrt{2S_{ij}S_{ij}} \end{cases} \tag{9}$$

Advantages
The realizable k-ε model has the immediate advantage of better predicting the spreading rate of both planar and round jets.
Furthermore, it performs better for flows that involve rotation, boundary layers subjected to severe adverse pressure gradients, separation, and recirculation [15].
Its equations help the results to fall back into the Lumley triangle, correcting the previous k-ε and k-ω models, that defines the non-variant flows in order to have a more accurate model [16].

Disadvantages
When the computational domain incorporates both rotating and stationary fluid as it happens here, one drawback is that it results in non-physical turbulent viscosities. This is because the realizable k-model defines the turbulent viscosity while taking the effects of mean rotation into account.
On systems with a single rotating reference frame, this additional rotation effect has been studied, and it has demonstrated superior performance over the traditional k-ε model. However, due to the nature of this alteration, attention is required when applying it to different reference frame systems [15].

IV. Spalart-Allmaras - SA

The one-equation Spalart-Allmaras turbulence model was created primarily for aerodynamic applications.
It is a low-Reynolds number model meaning that wall functions are not used [17] and the equation with which the turbulent eddy viscosity is calculated [18] is expressed in *Equation 10*.

$$\begin{cases} \dfrac{\partial \hat{\nu}}{\partial t} + u_j \dfrac{\partial \hat{\nu}}{\partial x_j} = c_{b1}(1 - f_{t2})\hat{S}\hat{\nu} - \left[c_{w1} f_w - \dfrac{c_{b1}}{\kappa^2} f_{t2}\right]\left(\dfrac{\hat{\nu}}{d}\right)^2 + \dfrac{1}{\sigma}\left[\dfrac{\partial}{\partial x_j}\left((\nu + \hat{\nu})\dfrac{\partial \hat{\nu}}{\partial x_j}\right) + c_{b2}\dfrac{\partial \hat{\nu}}{\partial x_i}\dfrac{\partial \hat{\nu}}{\partial x_i}\right] \\ \mu_t = \rho \hat{\nu} f_{v1} \end{cases} \tag{10}$$

Advantages
The computational efficiency is one of the main advantages of having a one-equation model. Moreover, for wall-bounded and unfavorable pressure gradient flows in boundary layers, the SA model is more accurate than the traditional k- model and useful as a low-Reynolds number model.

Disadvantages
On the other side, it lacks of information about the turbulence length scale and the transported quantity, the eddy viscosity, is just a model quantity and not a real one [19].

II. LES model

Wall-Adapting Local Eddy-viscosity subgrid-scale model - WALE SGS

The term "subgrid-scale modeling" describes the visualization of significant small-scale physical processes that take place at length-scales that are insufficiently defined on a computer mesh.
Subgrid-scale (SGS) modeling is used in large-eddy simulation of turbulence to mimic the impact of unresolved small-scale fluid motions (small eddies, swirls, and vortices) on the equations controlling the large-scale motions. These last, are solved in computer models [20].
In particular, the WALE model is an algebraic eddy viscosity model that considers rotations (see *Equation 11*) when calculating the μt (sub-grid scale eddy viscosity in *Equation 12*) and is able to handle transitions [21].

$$S_{ij}^{d} = \frac{1}{2}\left(\overline{g}_{ij}^{2} + \overline{g}_{ji}^{2}\right) - \frac{1}{3}\delta_{ij}\overline{g}_{kk}^{2} \tag{11}$$

Considering the sub-scale eddy viscosity as [22]:

$$\mu_t = \rho\Delta_s^2 \frac{(S_{ij}^{d}S_{ij}^{d})^{3/2}}{(\overline{S}_{ij}\overline{S}_{ij})^{5/2} + (S_{ij}^{d}S_{ij}^{d})^{5/4}} \tag{12}$$

Where $\overline{S_{ij}}$ is the rate-of-strain tensor for the resolved scale in *Equation 13*.

$$\bar{S}_{ij} = \frac{1}{2}\left(\frac{\partial \bar{u}_i}{\partial x_j} + \frac{\partial \bar{u}_j}{\partial x_i}\right) \tag{13}$$

Advantages

The key strength of this LES model is that is able to reproduce the laminar to turbulent transition.

Since the WALE model is sensitive to both the strain and the rotation rate of the small turbulent structures, its main advantage over the dynamic Smagorinsky model (one of the common possible options taken into account for LES simulations) is that the WALE model's formulation is based on the operators $S_{ij}^d S_{ij}^d$.

This makes it ideal for LES in complex geometries with structured or unstructured approaches, since only local information is necessary to create the eddy-viscosity and no explicit filtering is required [23].

Disadvantages

The main disadvantage of the WALE (and in general of LES) model is its high computational load, one needs to compute the problem in time in two stages: first to develop the flow, then to average the fields. Consequently, in our case it is employed only as a second confirmation of the results we already obtained with others RANS models.

4.1.1 Initial and boundary conditions

I. RANS models

Given the same initial conditions in the OpenFoam model, the accuracy of different RANS simulations was checked. Through all the different models, described in RANS turbulence models, the initial upstream condition were defined for several velocity magnitudes.

These conditions were computed using a turbulent boundary conditions calculator [24], considering as input parameters the initial speed, the turbulence intensity, the length scale, the characteristic length and the molecular viscosity.

Table 1 – Initial upstream conditions for the different RANS models

u[m/s] Initial speed	***ε[m^2/s^3] Turbulent dissipation***	***k[m^2/s^2] Turbulent kinetic energy***	***νt[m^2/s] Turbulent kinematic viscosity***	***ω[1/s] Turbulent dissipation rate***	***Re[-] Reynolds Number***
1	0.0002	0.015	0.082	0.122	6.67E+04
2	0.001	0.06	0.163	0.245	1.33E+05
5	0.021	0.375	0.408	0.612	3.33E+05
10	0.165	1.5	0.816	1.225	6.67E+05
15	0.558	3.375	1.225	1.837	1.00E+06
20	1.323	6	1.633	2.449	1.33E+06
25	2.583	9.375	2.041	3.062	1.67E+06
30	4.464	13.5	2.449	3.674	2.00E+06
40	10.582	24	3.266	4.899	2.67E+06

II. LES model

The LES simulation was applied to the U=1m/s because the RANS model was not converging properly at low speeds.
The initial conditions for the LES models were maintained constant through three simulations with different mesh resolutions:

- Inlet speed - U= 1 m/s
- Outlet pressure - p= 0 Pa (reconstructed flow)

Additionally, no other fluctuations were considered at the inlet of the mesh in order not to burden the already heavy computation, so all the turbulence is generated inside the domain.

4.1.2 Mesh considered

To compute the aerodynamic forces in the RANS and LES simulations, CFD computations have been carried out varying the orientation and relative speed of the wind.

The mesh has been generated using the cfmesh software [25] due to its fast computability and its robust workflows. It has been created by using mostly oct-tree refined hexahedral cells, except in the proximity of the body where body fitted polyhedral cells are created.

The domain has the following extents (in meters):

- x= [-2; 4]
- y= [-1.5; 1.5]
- z= [-1.5; 1.5]

Moreover, it is oriented using a pitch and yaw angle reference, to fix the position of the mesh in function of the desired orientation of the relative speed.
It was decided upon to maintain a constant orientation of the ice while manipulating the domain rotation to achieve various relative speed orientations. This approach allowed for the examination of different relative speed orientations without altering the ice's position.

The base position was taken at:

- roll_angle= 0° - rotation around the $\vec{x}_{axis}$
- pitch_angle= 0° - rotation around the $\vec{y}_{axis}$
- yaw_angle= 0° - rotation around the $\vec{z}_{axis}$

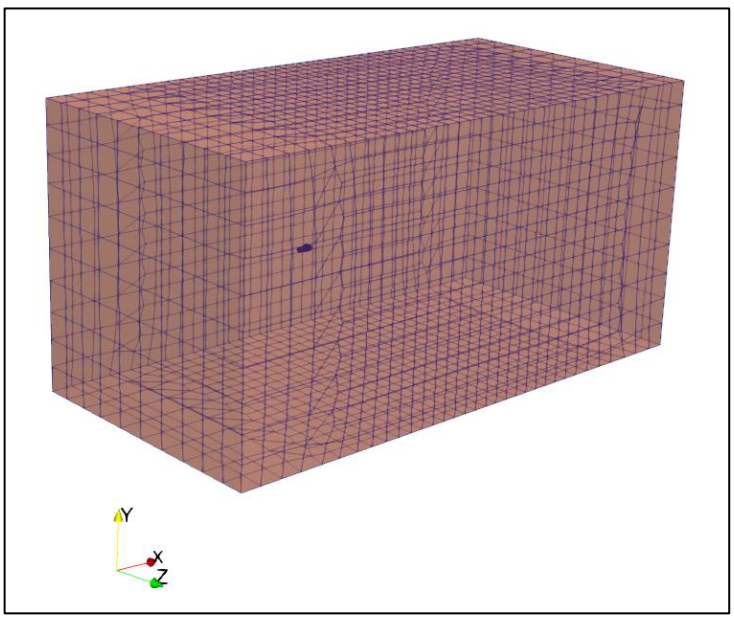

Figure 9 – Computational domain

4.2 Quality assurance

To verify the reliability of the problem set-up, this study started by validating the mesh used on the DAD ice shape. Both the mesh resolution and the domain size of the RANS and LES simulations have been varied to assure that the model taken would be the best one for the configuration chosen.

I. RANS sensitivity study

4.2.1 Mesh sensitivity study

The first parameter that has been studied was the number of cells taken, this was done to understand if they would be enough for the case considered. In order to do so, the mesh resolution on the coarsest level of the DAD ice shape has been varied from 0.7 m until the finest 0.1 m.

Figure 10 plots the total aerodynamic force as function of the solver iterations for the considered mesh resolutions. It can be observed that the chosen number of iterations is sufficient for the convergence.

To quantify this, the mean value of the normalized force between iterations 500-2000 has been compared to the mean in the interval 500-2500. The relative error is lower than 0,1% in all cases, meaning the force is almost constant after the 500^{th} value.

The most precise model would be the one described by the 0.1 mesh resolution but, due to its high computational cost, is not realistic to use it in our study. Moreover, it is the least stable one, as it is clearly displayed in *Figure 10* (F_0.1).

The best mesh resolution would be one in which we have no fluctuation but still a high reliance. Therefore, the 0.3 mesh resolution model has been picked (F_0.3) since the predicted force is practically the same as on the next finer mesh level (F_0.2).

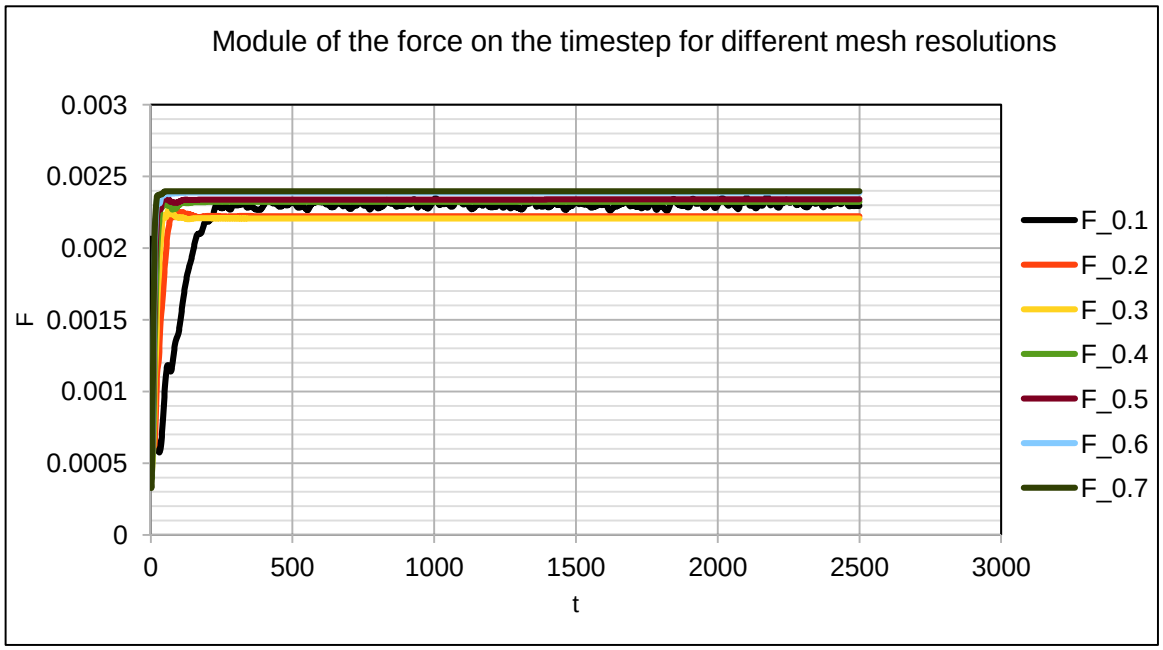

Figure 10 – Module of the force for different mesh resolutions

4.2.2 Sensitivity study of the wall function y^+

To study the performance of the turbulence models in 4.1 Model description near the wall, the aerodynamic force, being an integral quantity, might not be sufficient to assess grid sensitivity.
In fact, some established turbulence models, such as k-ε; are only applicable where the turbulence is fully developed and do not function well near walls. In this particular area, we need to assess the grid resolution.
Commonly the grid resolution is normalized and is expressed in terms of y^+,

$$y^+[-] = \frac{y \cdot u_\tau}{\upsilon} \quad (14)$$

Considering:

- u_τ - friction velocity
- y - the absolute distance from the wall
- υ - kinematic viscosity

If y^+ is around 1 or smaller, the grid resolution is sufficient to resolve the boundary layer. For larger values (but less than ca. 100-150) wall functions are needed. For even larger values the grid is deemed too coarse.

Therefore, after investigating this parameter, the results show that, at low speed, U=1 m/s the normalized wall distance is y^+=0.3; while when the velocity is increased to U=30-40 m/s, the value increases to y^+=45-54 as pictured in *Figure 11*.

Taking into consideration that the mean value of $y^+ \cong$10-15, the grid resolutions used can be considered accurate enough; in fact, to have a wrong model y^+ should reach at least 150.

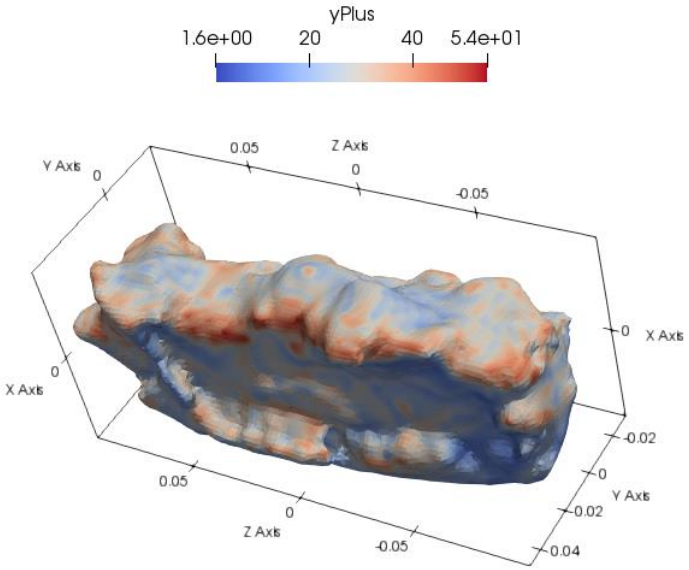

Figure 11– Distribution of y+ in the DAV ice concretion

4.2.3 Domain size sensitivity

Furthermore, the overall dimension of the domain used has been taken into consideration. To prove its trustworthiness, both a diminished (25% smaller than the base case) and an expanded mesh (25% bigger than the standard scenario) of the DAD ice shape were considered, resulting in a sufficiently sized mesh for our study.

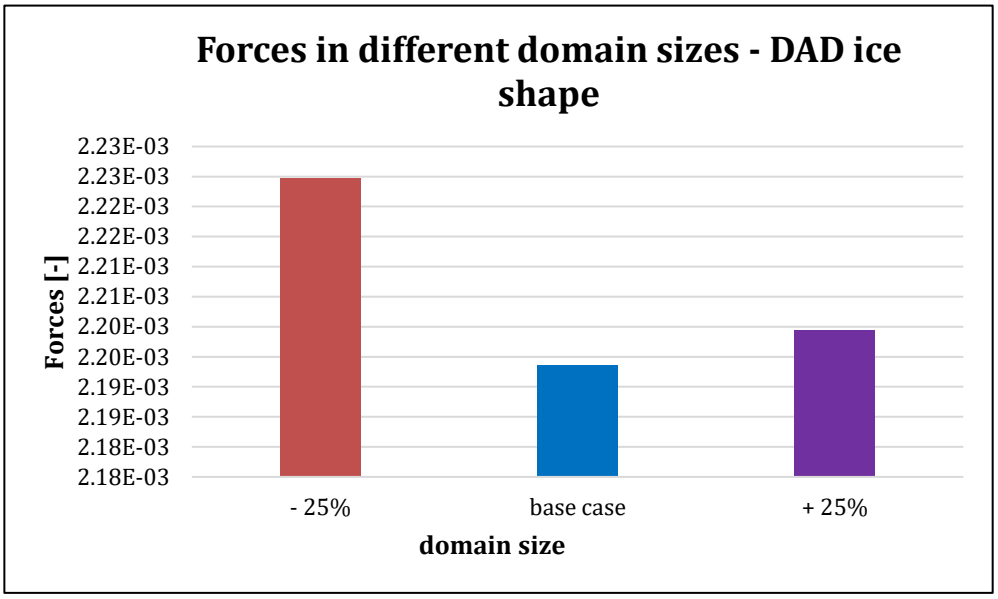

Figure 12 – Comparison of different mesh dimensions considering the DAD ice shape

More specifically, there is barely any difference between the three mesh dimensions from the simulations' results point of view, having a relative error of 0.269% for the bigger mesh and 1.406% for the smaller one.

4.2.4 Comparison with the data of Drapalik

The picked mesh has been oriented in the six main directions in order to compare if the force values predicted by Drapalik et al.[7] could be reproduced. Two speeds have been considered, 1 m/s and 2m/s.
As it can be observed from *Table 2* and *3*, the error in between the predicted forces and the computed ones is overall lower than 30% so the results can be taken as reliable.

Table 2– Force computations for U= 1m/s

DAV U=1m/s	***F_Drapalik***	***F1-6***	***error***
+x	0.0066	0.0049	24.95%
-x	0.0061	0.0044	27.66%
+y	0.0073	0.0056	23.60%
-y	0.0083	0.0061	26.65%
+z	0.0016	0.0012	23.62%
-z	0.0015	0.0012	21.97%

Table 3 – Force computations for U= 2m/s

DAV U=2m/s	***F_Drapalik***	***F1-6***	***error***
+x	0.0244	0.0192	20.97%
-x	0.0234	0.0168	27.89%
+y	0.0270	0.0213	21.35%
-y	0.0305	0.0233	23.67%
+z	0.0059	0.0047	20.86%
-z	0.0055	0.0044	20.15%

II. LES sensitivity study

For the LES case, the mesh resolution has been varied in between three different resolutions, increasingly refining the size of cells near the object.
Starting with the first mesh with the lowest resolution of 1.96E+06, then it has been increased to 6.09E+07 and the final number of cell of the last mesh was assessed to be 1.36E+07. In *Figure 13* it is depicted the behavior of the force in function of the mesh resolution and the error bars indicate the RMS of the forces.

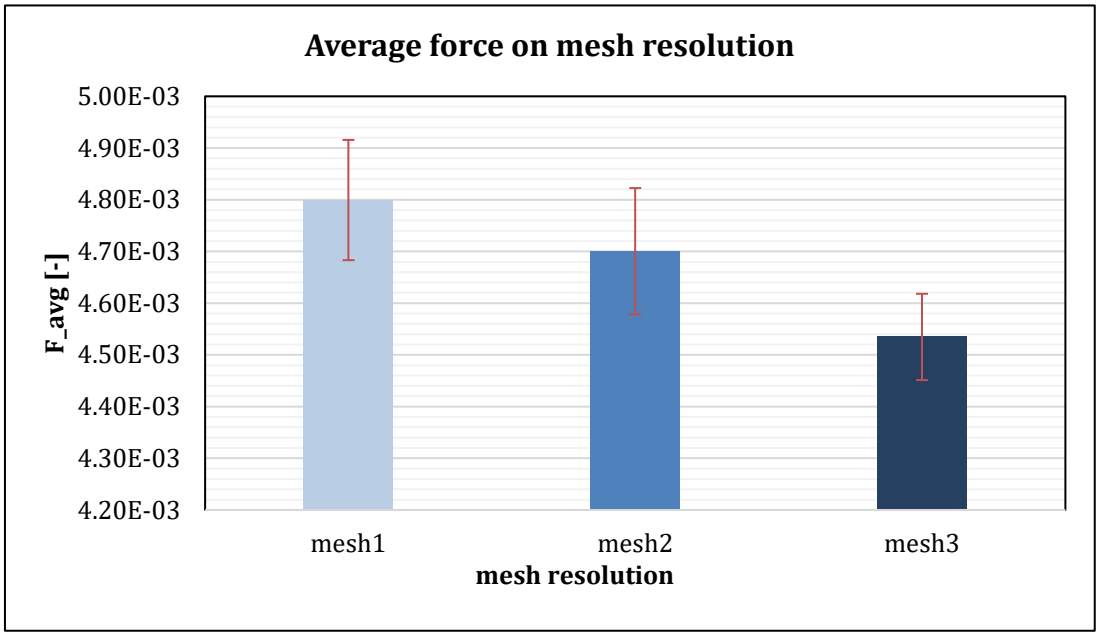

Figure 13– Comparison of the effect of different mesh resolution on the average force in the LES simulations

As we can see, the forces decrease while increasing the mesh resolution. If the simulation wouldn't have been so expensive, a possible improvement could have been testing an even finer mesh.

To be able to compare the change in the behaviour of the speed in function of the accuracy of the mesh, seven different probes point were placed in the wake area and its speed and force values were studied (*Figure 14*). In particular, for point 4 (0.127; 0.0253;0) the behaviour of the instantaneous speed in the three mesh-case scenarios was investigated.

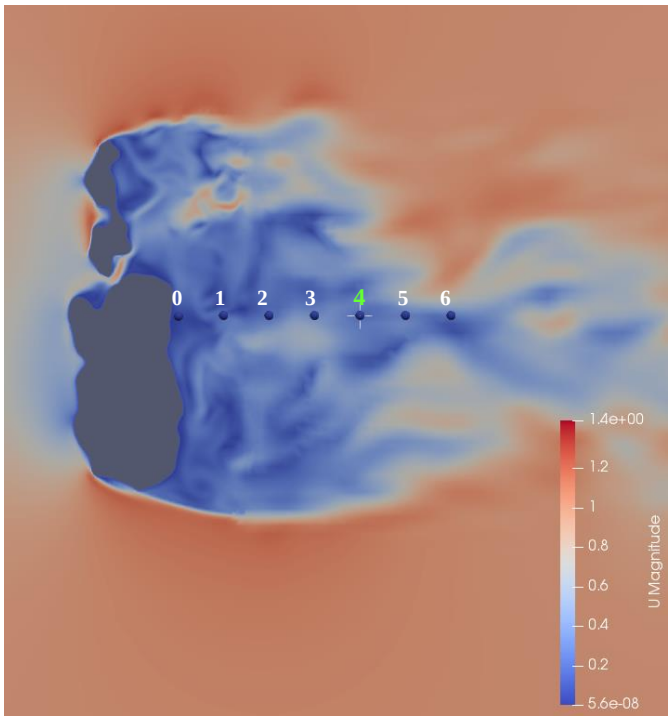

Figure 14– Probes position in the wake area

Then, it has been plotted the specific kinetic energy (proportional to the square of the fluctuation speed) in function of the frequency of the system using a double-logarithmic scale to compare the results with the energy cascade model.
As outlined in *Figure 15*, as soon as the resolution of the mesh is increased, the model gains precision, covering a larger interval in the inertial subrange ($k^{-\frac{5}{3}}$ in the legend).

Up until f $\cong 10^2$, the results follow the tendency of the Kolmogorov scale profile, depicted as the theoretical tendency in the dashed line in *Figure 15*.

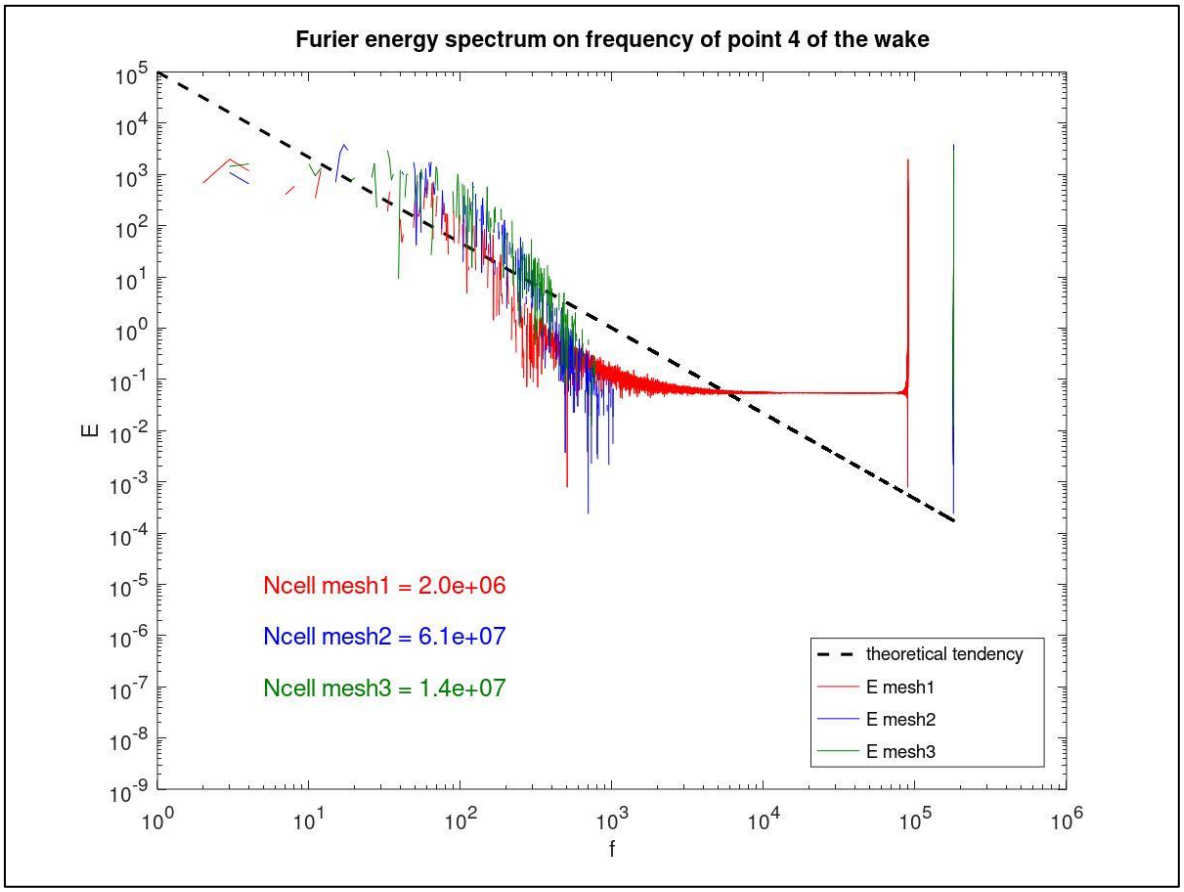

Figure 15– Comparison of the meshes and the number of cells for the LES simulations of point 4 of the wake over the entire frequency range

Whereas, for higher frequencies, the numerical error dissipates the energy too fast so is not relevant to the physical analysis, this is the reason why in *Figure 16* the attention is focused only in the initials frequency area.

This behaviour is explained from the experimental relation in between the LES computational cost and the turbulence Reynolds number: $N_{LES} \sim Re_\tau^2$, with $Re_\tau = \frac{U' \cdot L}{\upsilon}$, having U' the fluctuation velocity, L=0.2 m, the scale of the system and $\upsilon = 10^{-5}$, the viscosity.

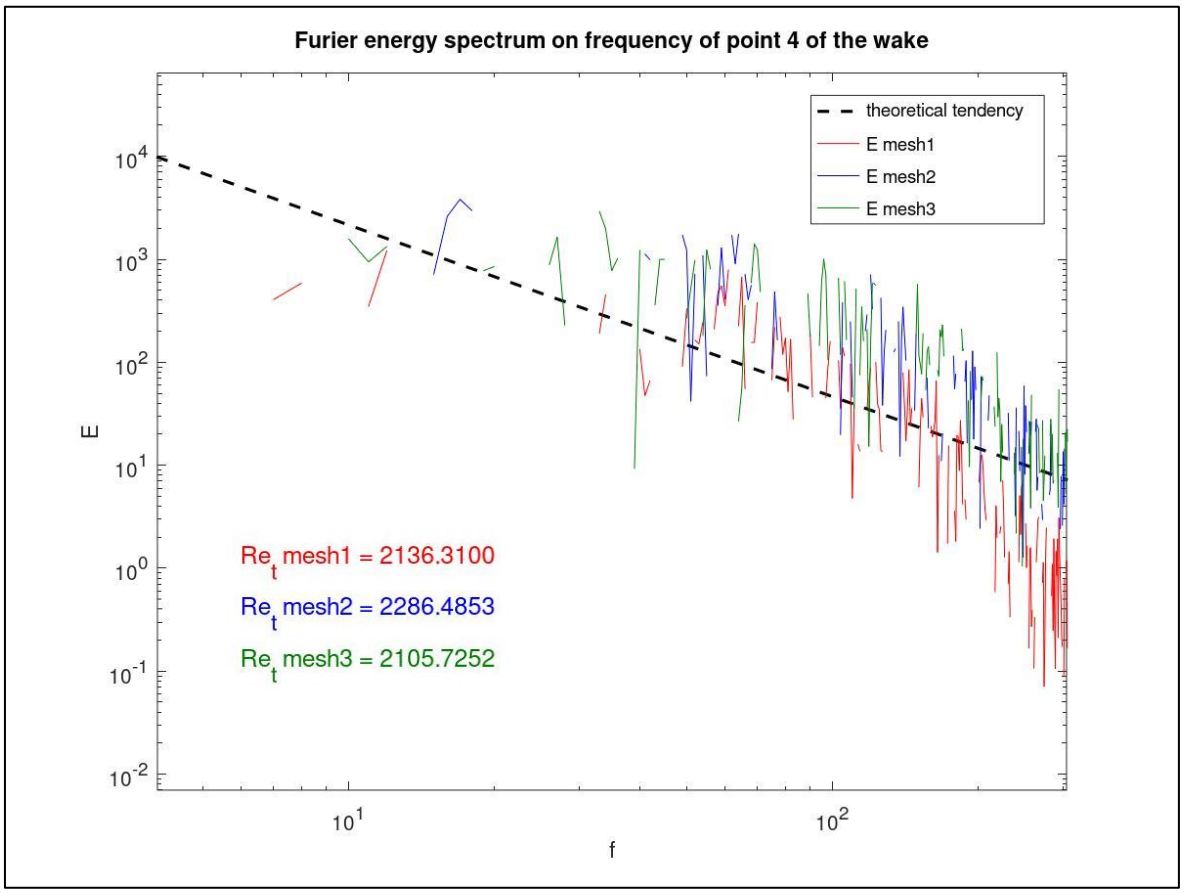

Figure 16 – Comparison of the meshes and the Reynolds turbulent numbers for the LES simulations of point 4 of the wake for the initial frequency

4.3 Results

I. RANS models comparisons

Figure 17 plots the predicted normalized forces for all the RANS models considered in this study while increasing the velocity.

As it was expected, the Realizable k-ε model is the one with the highest incompatibility due to its generation of non-physical turbulent viscosities, as explained in the Realizable model; the second worst is the RNG one as depicted, since it increases the effects of small vortexes turbulences.

On the other hand, the SST model (Fx_SST) and the Spalart Allmaras model (Fx_SA) describe better the behaviour of the forces on the ice. Regarding SA and SST, due to the comparable predictions made by these two models, there is a high probability that they are calculating accurate values.

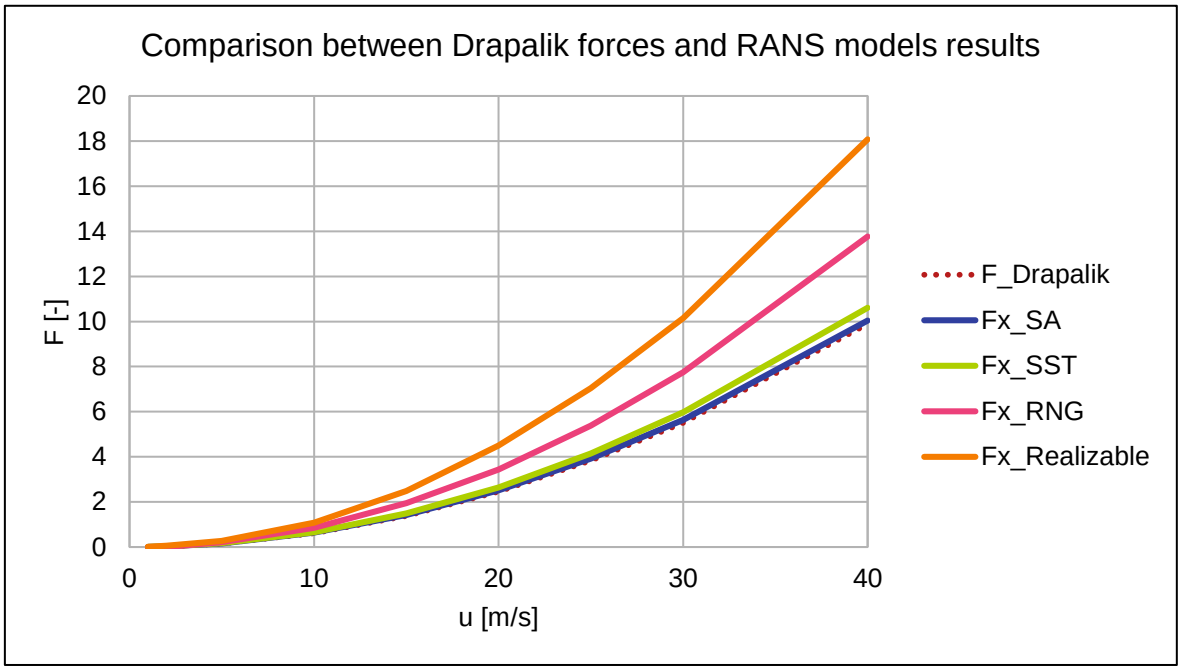

Figure 17 – Comparison in between the forces predicted by the different RANS models

II. LES model comparison

In a second step of the analysis, the LES simulations were carried out to double test the results from the RANS simulations in the less reliable case, at U=1m/s.

Due to the high computation costs, only three different LES simulation were completed, in which the refinement of the mesh was modified. In the first one, the simulation was developed for 10 s and then averaged for other 10, while the second and the third were averaged starting from the 10th second of the first simulation and for 10s more, in order to save some computational time.
As depicted in *Figure 18*, for the finest mesh case scenario, the chaotic vortexes structures increases in the wake area.

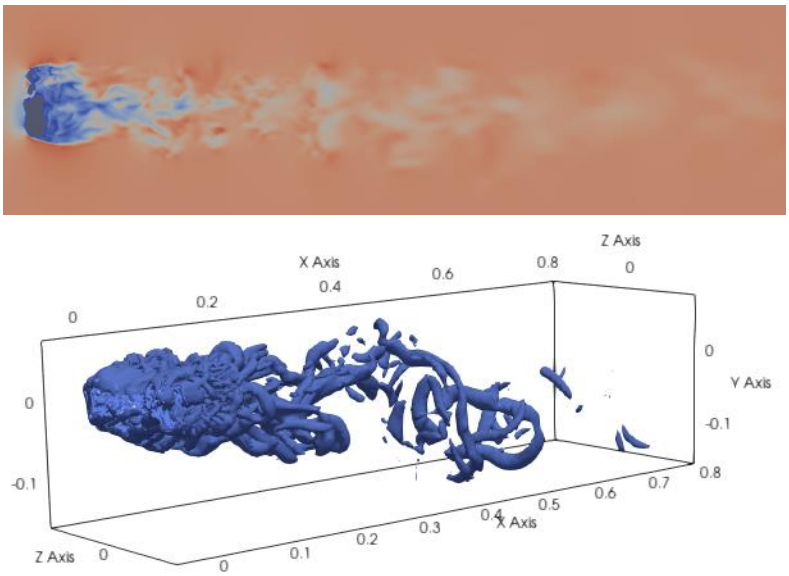

Figure 18 – Resolution of the instantaneous velocity field (up figure) and structures (down figure) of the turbulent vortexes for DAV ice shape at U=1m/s

Later on, in the comparison of the results for the first LES mesh and the SST-k-ε model in *Figure 19*, it is evident that the velocity field is not entirely described by the RANS simulations, making the more accurate LES simulations necessary. In fact, in the figure on the right, the prevalence of vortexes is growing, signalling the need for a more detailed research.

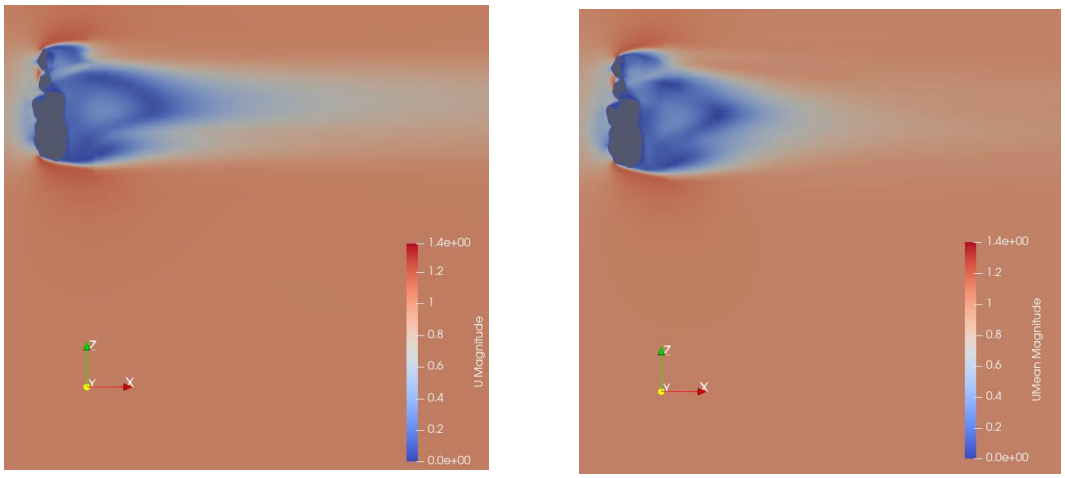

Figure 19– Comparison between the module of the speed in the SST-k-ε model (on the left) and the averaged speed in the LES model (on the right).

It can be stated the same for the forces, in the LES resolution the value of the normalized mean force is F_{LES_mesh1}= 4.80E-03; while for the RANS F_{RANS_SST}=6.64E-03. Consequently, the relative error in the evaluation of the force is considerable, around 40%.

This results repeats also for the kinetic energy that varied more than depicted in the RANS model in *Figure 20* (figure on the left).

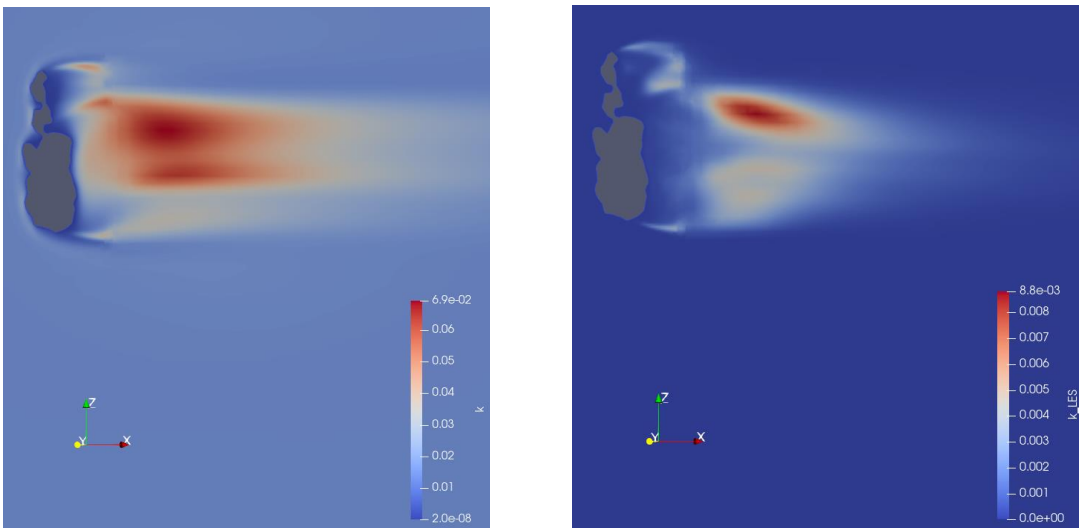

Figure 20– Comparison between the kinetic energy in the SST-k-ε model (on the left) and in the LES model (on the right).

In conclusion, refining the mesh helps to identify more turbulences after the body considered.

4.4 Conclusions

Reminding that, the Reynolds-Averaged Navier-Stokes simulations are an average analysis of the turbulent flow, while Large Eddy Simulations are more accurate even if they still ignore the smallest length scales, which are the most computationally expensive to resolve, the following conclusions can be drown.

For the RANS simulations, it has appeared that the k-ω SST model and the Spalart-Allmaras model (SA) are highly effective compared to the Re-normalization group (RNG) and the Realizable model. In particular, the Spalart-Allmaras model had proved to be a cost-efficient option and is likely sufficient for future computations.

As said before, the force value is different in between the RANS and LES simulations, so, depending on the level of accuracy that is needed in the situation considered, it would be better to work with one or the other. Nevertheless, in cases where convergence issues arise or there is a sudden change in magnitude, is prudent to double checked the results using LES.

5. Sensitivity of the trajectories

5.1 Model description

At this point, the forces acting on the ice concretion were analysed with the model developed in OpenFoam and compared with the Drapalik study results [7].

Starting from the in-house ballistic model (LU) the trajectories of the ice falling were evaluated. This model differentiates from the one used by Drapalik et al.[6] in having a 6 DOF system, by way of taking into account the rotation of the ice, and considering the damping effect of forces.

Then, the model was applied, considering the initial data in *Table 4*, to create a hypothetical trajectory in order to be able to predict where the ice will fall.

Finally, a map of the probable impact points was created and the different results were compared to find the most accurate model description.

5.1.1 Initial conditions

To set the initial data the following mesh has been created to simplify the work:

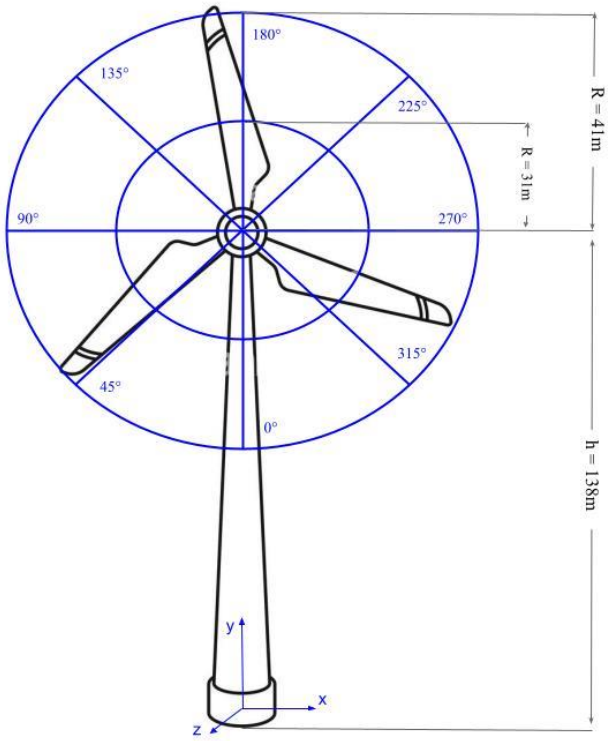

Figure 21 – Problem set-up used to study the trajectories

As shown in *Figure 21*, the ice trajectories have been computed for eight different azimuthal starting position of the rotor blade. In radial direction, we considered only two positions in the computations, 31 and 41 m, however the focus in the following observations will be on the 41 m case, since that is the radial position discussed in [6].

A summary of the set-up is shown in *Table 4*. For the incoming wind velocity, the same logarithmic profile has been used as in [6].

Table 4 – Initial conditions of the trajectory simulation

	x	**y**	**z**
WT Rotor position [m]	138		
WT Rotor axis [-]	0	0	1
WT Rin [m]	31		
WT Rout [m]	41		
NR	2		
WT omega [rpm],	0		
Nazimuthal	8		
Wind speed specification method (1- constant; 2-logaritmical)	2		
Surface roughness length [m]	0.05		
Air density [kg/m^3]	1.276		
mObj [kg]	0.282		
Iobj [kg m^2]	0.01222	0.01222	0.00564
Lengthscale [m]	0.2		

5.1.3 Aerodynamic force and momentum database

In the in-house solver used for the trajectory computations, the forces and the moments are normalized by the relative velocity magnitude. As such, the database depends only on the orientation of the relative velocity.

Thus, it can be imagined that the data is stored in an imaginary unit sphere. Since each data-point is obtained by CFD, it would be preferred to optimize the force database to minimize the number of CFD computations.

In this section, the impact of the database density on the predicted ice trajectories is investigated. The mesh taken is a quasi-triangular one, taken on the unit sphere surface.

The coarsest one has been created by taking the middle point of the intersection of the sphere with the axes, so to have 6 total points (see *Figure 22*).

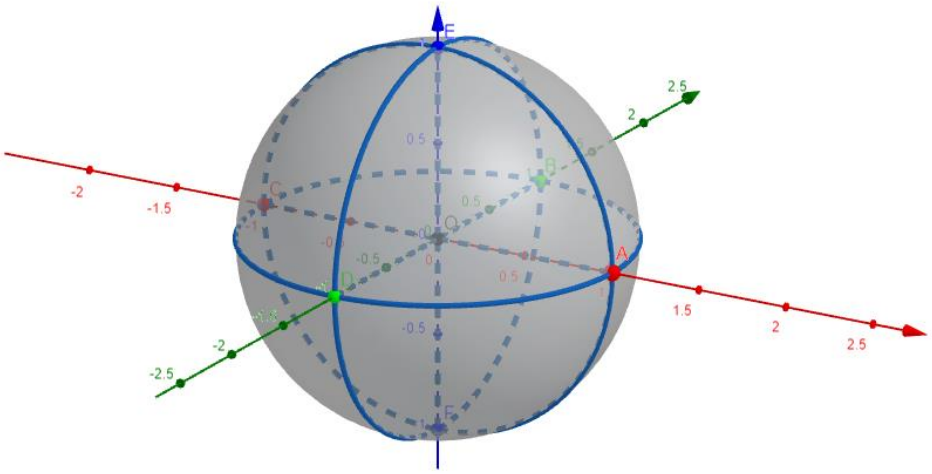

Figure 22 – Initial spherical mesh considered

After, the mesh was refined by dividing each edge at the midpoint, resulting in 18 (on the medium) and 66 (on the finest) data-points, like illustrated in *Figure 23.* The force and momentum values were taken from [6].

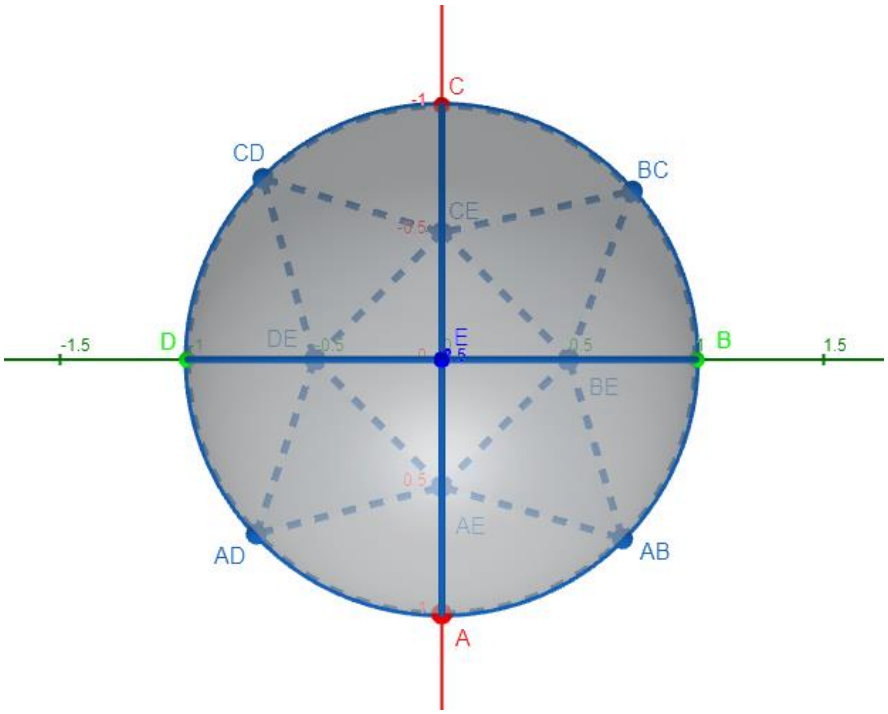

Figure 23 – Second division in 18 points, section y-x of the spherical mesh

5.2 Results

I. Simulations carried out at different mesh refinements

As said before, three simulations has been considered while gradually increasing the accuracy of the mesh. The initial spherical mesh has been divided in 6 main points (mesh1), from which the results has been interpolated; they have later been increased to 18 (mesh2) and ultimately to 66 (mesh3), giving different results.

As soon as the refinement of the mesh considered is increased to study the impact points, the throwing distance decreased. In the trajectory computations, the instantaneous forces and moments acting on the ice are determined using an inverse-distance interpolation to the three closest available data-points.

As expected, the change from using the coarsest (in red in *Figure 24*) to the medium mesh (in blue in *Figure 24*) has a huge influence on the impact positions. Comparing the results for the medium and fine mesh (in green in *Figure 24*), the predicted impact positions are much closer to each other, but there are still visible differences.

Hence, the best choice would be the last mesh picked, mesh3, being the most accurate one and noticing so different results with the other two.

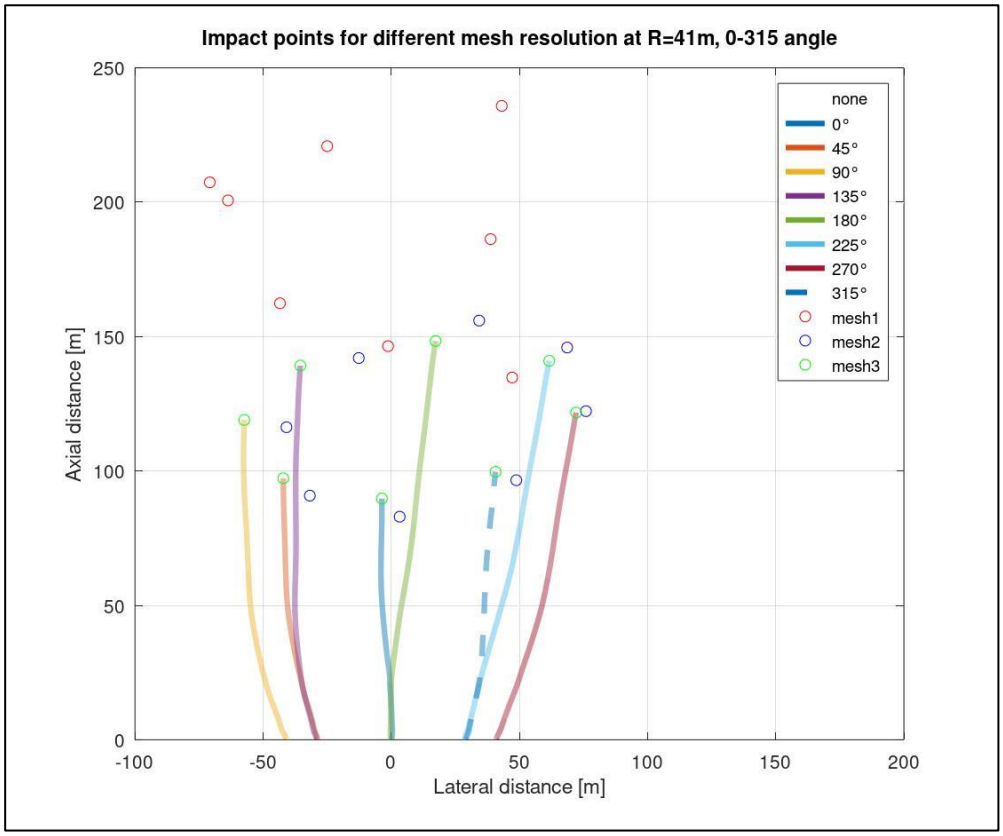

Figure 24 – Comparison of the falling point considering different mesh resolutions

II. Force accuracy study

When determining the force and momentum database, there are several error sources: mesh resolution, initial and boundary conditions, solution methods, steady assumption of the ice, etc.; thus, it would be interesting to know the effect of errors of a certain magnitude on the trajectories.
Consequently, to study the accuracy of the forces considered, an additional analysis was conducted simulating a Monte Carlo study. Error magnitudes ranging from 1% to 50% were introduced, and each error level was subjected to 100 computational trials to assess the effects of error fluctuations. This additional accuracy study has been implemented to take into account the possibility of random fluctuations of the force and momentum coefficients read from the database.

And so, as a final check for the forces considered:

$$\boldsymbol{F_{final}} = [F_{database} \cdot (1 - p + 2 \cdot RND01 \cdot \mathrm{p})] \tag{15}$$

as:

- $F_{database}$ - force/momentum read from the database
- $p = [0.01, 0.05, 0.1, 0.25, 0.5]$ - error magnitude that varies from 1% up to 50%
- $RND01$ - random number between 0 and 1

It should be stressed that the experiments' random fluctuations might not be exactly comparable for actual mistakes; however, determining a rough estimate of the order of magnitude is the analysis's main goal.

As depicted in *Figure 25*, as the error magnitude increases, the average force database loses its reliability.

So for p<0.1, the relative error between the value of the force database with the lowest fluctuation ($F_{@p=0.01}$) and the other forces calculated ($F_{@p=[0.05,0.1]}$) is lower than 20%, while for p=0.25 and 0.5, subsequently, the relative error increases until it reaches peaks of 70%.

From a more meaningful point of view, this means that, if the fluctuation of the force considered is low, the final impact point will have an impact error of the magnitude of maximum one meter, so an acceptable error, considering the total throwing distance around 100m. On the other hand, if the variation increases the imprecision can reach 8-9 m.

To put it in perspective, considering that a car has a length of about 4m, the model is wrong about two cars and it starts to be dangerous for realistic implementations.

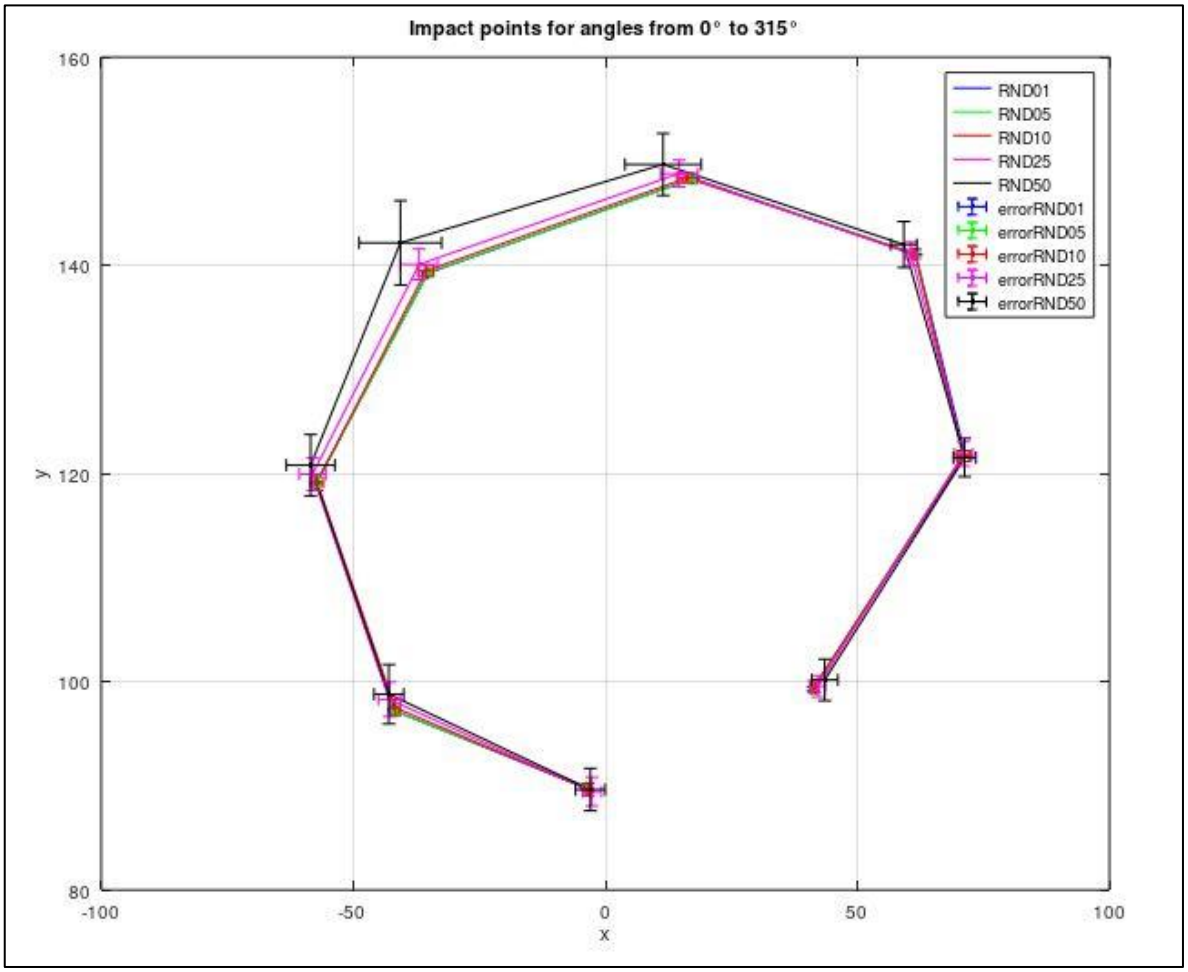

Figure 25 – Results of the fluctuation study

5.3 Conclusions

In conclusion, to improve the aerodynamic forces and momentum database using a refinement approach, the trajectory computations for ice concretions were completed.

In this trajectory sensitivity study, several mesh improvements were analysed, and the effects of error magnitudes on force predictions were assessed. The outcomes showed that increasing mesh refinement increased the impact position accuracy, and, actually, the finest the mesh generated, the most accurate the results.

Additionally, the review of error magnitudes showed how they had a big impact on the averaged force database reliability, with bigger error magnitudes resulting in larger departures from predicted values.

This work advances knowledge of ice trajectory predictions by using refining approaches and provides insights into how the database correctness affects force estimates.

6. Discussion and future plans

In summary, this paper offers insightful information that will be useful for further work. Regarding the results for the Reynold number effect, it can be deduced that the single unit sphere is insufficient to properly represent the complicated dynamics for low flow velocities. Therefore, to take into account the Re-dependence and assure reliable findings, using multiple unit spheres in future analyses would be the optimal approach, for obtaining more trustworthy results.

Whereas, in relation to the turbulence model, the k-ω SST and SA models have both showed potential for turbulence modeling, but, being a cost-effective choice, SA is probably enough for upcoming calculations due to the single equation that characterizes it.
However, it is always advisable to cross-validate the results using the LES as a reference in circumstances when convergence problems or abrupt changes in magnitude occur.

Finally, for the trajectories sensitivity, the use of the uniform mesh refining approach for the aerodynamic force and momentum database, has improved the accuracy for the trajectory computations. In the future, it would be interesting to study a tree-based refinement approach to verify the accuracy of the results previously obtained and to refine the precision of the impact points.

In conclusion, these outcomes have important ramifications for both theoretical and practical researches. Re-dependence, proper turbulence models and advanced trajectory computation techniques, can contribute to help researchers improve the precision and dependability of their findings. This study lays the preliminary investigations for future advances in understanding fluid dynamics and makes significant recommendations for future research in related domains.

7. References

[1] Makkonen, Lasse & Laakso, Timo & Marjaniemi, Mauri & Finstad, Karen. (2001). Modelling and Prevention of Ice Accretion on Wind Turbines. Wind Engineering. 25. 3-21. 10.1260/0309524011495791

[2] Arash Raeesi, Sean McTavish, Annick D'Auteuil, *Aerodynamic characteristics of generic ice shells*, Journal of Wind Engineering and Industrial Aerodynamics, Volume 184, 2019, Pages 49-60, ISSN 0167-6105, https://doi.org/10.1016/j.jweia.2018.11.002

[3] Szász, R.-Z.; Leroyer, A.; Revstedt, J., *Numerical Modelling of the Ice Throw from Wind Turbines*. Int. J. Turbomach. Propuls. Power 2019, 4, 4. https://doi.org/10.3390/ijtpp4010004

[4] Biswas, S., Taylor, P. and Salmon, J. (2012), A *model of ice throw trajectories from wind turbines. Wind Energ.*, 15: 889-901. https://doi.org/10.1002/we.519

[5] Markus Drapalik, Larissa Zajicek, Sebastian Purker, *Ice aggregation and ice throw from small wind turbines*, Cold Regions Science and Technology, Volume 192, 2021, 103399, ISSN 0165-232X, https://doi.org/10.1016/j.coldregions.2021.103399

[6] Markus Drapalik, *Site-specific simulation of ice shed and ice throw from wind turbines using ballistic models* (EISBALL), 2021, http://www.risk.boku.ac.at/en/forschung/forschungsschwerpunkte/erneuerbare-energie/eisball/

[7] Sebastian Purker, *Meshing komplexer Eisstrukturen für die Simulation von Eisfall und Eiswurf von Windkraftanlagen*, 2022, Institute for Safety and Risk Sciences Department of Vasser-Atrnosphare-Urnwelt

[8] OpenFOAM (Version 10), 2004, Retrieved from www.openfoam.org (Accessed 03-04.2023)

[9] simpleFoam documentation, Retrieved from https://www.openfoam.com/documentation/guides/latest/doc/guide-applications-solvers-incompressible-simpleFoam.html (Accessed 03.2023)

[10] pimpleFoam documentation, Retrieved from https://www.openfoam.com/documentation/guides/latest/doc/guide-applications-solvers-incompressible-pimpleFoam.html (Accessed 03.2023)

[11] Christopher Rumsey, *The Menter Shear Stress Transport Turbulence Model*, Turbulence Modeling Resource, 2021, https://turbmodels.larc.nasa.gov/sst.html

[12] Jade M, *Use of k-epsilon and k-omega Models*, 2010, https://www.cfd-online.com/Forums/main/75554-use-k-epsilon-k-omega-models.html

[13] CFD online, *RNG k-epsilon model*, https://www.cfd-online.com/Wiki/RNG_k-epsilon_model

[14] CFD online, *Realisable k-epsilon model*, https://www.cfd-online.com/Wiki/Realisable_k-epsilon_model

[15] University of Washington, *Modeling Turbulence*, 2006, https://courses.washington.edu/mengr544/handouts-10/Fluent-k-epsilon.pdf

[16] M.Emory and G.Iaccarino, *Visualizing turbulenc eanisotropy in the spatial domain with componentality contours*, 2014 https://web.stanford.edu/group/ctr/ResBriefs/2014/14_emory.pdf

[17] Comsol, *The Spalart-Allmaras Turbulence Model*, https://doc.comsol.com/5.5/doc/com.comsol.help.cfd/cfd_ug_fluidflow_single.06.093.html#:~:text=The%20Spalart%2DAllmaras%20turbulence%20model%20is%20a%20one%2Dequation%20turbulence,wall%20where%20viscous%20effects%20dominate.

[18] Christopher Rumsey, *The Spalart-Allmaras Turbulence Model*, 2023, https://turbmodels.larc.nasa.gov/spalart.html

[19] Altair Community, *What are the advantages and disadvantages of the Spalart-Allmaras model?*, 2013, https://community.altair.com/community?id=community_question&sys_id=f596c07a1b2bd0908017dc61ec4bcb14

[20] Prof. Charles Meneveau, Johns Hopkins University, *Turbulence: Subgrid-Scale Modeling*, http://www.scholarpedia.org/article/Turbulence:_Subgrid-Scale_Modeling

[21] CFD WITH A MISSION, *WALE SGS model in OpenFOAM*,, 2019, https://caefn.com/openfoam/wale-sgs-model

[22] CFD online, *Wall-adapting local eddy-viscosity (WALE) model, https://www.cfd-online.com/Wiki/Wall-adapting_local_eddy-viscosity_(WALE)_model*

[23] F. Piscaglia, A. Montorfano, A. Onorati, F. Brusiani, *Boundary Conditions and SGS Models for LES of Wall-Bounded Separated Flows: An Application to Engine-Like Geometries*, Oil&Gas Science and Technology - Revue d'IFP Energies nouvelles, 2014, 10.2516/ogst/2013143 / hal-01933365

[24] Turbulent boundary conditions calculator, Retrieved from https://cfd-training.com/turbulent-boundary-conditions-calculator/ (Accessed 04.2023)

[25] CF-MESH+®, 2023, Retrieved from https://cfmesh.com/ (Accessed 03-04.2023)

Annex I

I. RANS MODELS

fvSchemes RANS

```
/*---------------------------------*- C++ -*----------------------------------*\
  =========                 |
  \\      /  F ield         | OpenFOAM: The Open Source CFD Toolbox
   \\    /   O peration     | Website:  https://openfoam.org
    \\  /    A nd           | Version:  7
     \\/     M anipulation  |
\*---------------------------------------------------------------------------*/
FoamFile
{
    version     2.0;
    format      ascii;
    class       dictionary;
    object      fvSchemes;
}
// * * * * * * * * * * * * * * * * * * * * * * * * * * * * * * * * * * * * * //

ddtSchemes
{
    default         steadyState;
}

gradSchemes
{
    default         Gauss linear;
    grad(U)         cellLimited Gauss linear 1;
}

divSchemes
{
    default         none;
    div(phi,U)      bounded Gauss linearUpwindV grad(U);
    div(phi,k)      bounded Gauss upwind;
    div(phi,omega)  bounded Gauss upwind;
    div((nuEff*dev2(T(grad(U))))) Gauss linear;
}
```

```
laplacianSchemes
{
    default         Gauss linear corrected;
}

interpolationSchemes
{
    default         linear;
}

snGradSchemes
{
    default         corrected;
}

wallDist
{
    method meshWave;
}


//
// ************************************************************************* //
```

fvSolution RANS

```
/*--------------------------------*- C++ -*----------------------------------*\
  =========                 |
  \\      /  F ield         | OpenFOAM: The Open Source CFD Toolbox
   \\    /   O peration     | Website:  https://openfoam.org
    \\  /    A nd           | Version:  7
     \\/     M anipulation  |
\*---------------------------------------------------------------------------*/
FoamFile
{
    version     2.0;
    format      ascii;
    class       dictionary;
    object      fvSolution;
}
// * * * * * * * * * * * * * * * * * * * * * * * * * * * * * * * * * * * * * //
```

```
solvers
{
    p
    {
        solver          GAMG;
        smoother        GaussSeidel;
        tolerance       1e-7;
        relTol          0.01;
    }

    Phi
    {
        $p;
    }

    U
    {
        solver          smoothSolver;
        smoother        GaussSeidel;
        tolerance       1e-8;
        relTol          0.1;
        nSweeps         1;
    }

    k
    {
        solver          smoothSolver;
        smoother        GaussSeidel;
        tolerance       1e-8;
        relTol          0.1;
        nSweeps         1;
    }

    omega
    {
        solver          smoothSolver;
        smoother        GaussSeidel;
        tolerance       1e-8;
        relTol          0.1;
        nSweeps         1;
    }
}
```

```
SIMPLE
{
    nNonOrthogonalCorrectors 0;
    consistent yes;
}

potentialFlow
{
    nNonOrthogonalCorrectors 10;
}

relaxationFactors
{
    equations
    {
        U               0.9;
        k               0.7;
        omega           0.7;
    }
}

cache
{
    grad(U);
}

//
************************************************************************
//
```

II. LES MODELS

fvSchemes LES

```
/*---------------------------------*- C++ -*----------------------------------*\
| =========                 |                                                 |
| \\      /  F ield         | OpenFOAM: The Open Source CFD Toolbox           |
|  \\    /   O peration     | Version:  v2106                                 |
|   \\  /    A nd           | Website:  www.openfoam.com                      |
|    \\/     M anipulation  |                                                 |
\*---------------------------------------------------------------------------*/
```

```
FoamFile
{
    version     2.0;
    format      ascii;
    class       dictionary;
    object      fvSchemes;
}
// * * * * * * * * * * * * * * * * * * * * * * * * * * * * * * * * * * * * * * * * * * * * //

ddtSchemes
{
    default         backward;
}

gradSchemes
{
    default         Gauss linear;
}

divSchemes
{
    default         none;

    div(phi,U)      Gauss LUST grad(U);

    div(phi,nuTilda) Gauss limitedLinear 1;

    div(phi,k)      Gauss limitedLinear 1;

    div((nuEff*dev2(T(grad(U))))) Gauss linear;
}

interpolationSchemes
{
    default         linear;
}

laplacianSchemes
{
    default         Gauss linear corrected;
}
```

```
snGradSchemes
{
   default         corrected;
}

wallDist
{
   method          meshWave;
}


//
// ************************************************************************* //
```

fvSolution LES

```
/*--------------------------------*- C++ -*----------------------------------*\
| =========                 |                                                 |
| \\      /  F ield         | OpenFOAM: The Open Source CFD Toolbox           |
|  \\    /   O peration     | Version:  v2106                                 |
|   \\  /    A nd           | Website:  www.openfoam.com                      |
|    \\/     M anipulation  |                                                 |
\*---------------------------------------------------------------------------*/
FoamFile
{
   version     2.0;
   format      ascii;
   class       dictionary;
   object      fvSolution;
}
// * * * * * * * * * * * * * * * * * * * * * * * * * * * * * * * * * * * * * * * * //

solvers
{
   p
   {
      solver          GAMG;
      smoother        DICGaussSeidel;
      tolerance       1e-20;
      relTol          0.05;
   }
```

```
    pFinal
    {
        $p;
        tolerance       1e-6;
        relTol          0;
    };

    "(U|nuTilda|k)"
    {
        solver          PBiCGStab;
        preconditioner  DILU;
        tolerance       0;
        relTol          0.1;
    }

    "(U|nuTilda|k)Final"
    {
        $U;
        tolerance       1e-6;
        relTol          0;
    }
}

PIMPLE
{
    nOuterCorrectors 1;
    nCorrectors     2;
    nNonOrthogonalCorrectors 1;
    transonic       no;
    consistent      no;
}

PISO
{
    nCorrectors     2;
    nNonOrthogonalCorrectors 0;
    pRefCell        0;
    pRefValue       0;
}


relaxationFactors
```

```
{
    nuTilda         0.8;
    U               0.8;
    p               0.8;
    ".*Final"       1.0;
}


//
********************************************************************************
//
```